Global Change Biology

Global Change Biology (2014) **20**, 594–606, doi: 10.1111/gcb.12391

Vegetation controls on northern high latitude snow-albedo feedback: observations and CMIP5 model simulations

MICHAEL M. LORANTY*†, LOGAN T. BERNER*, SCOTT J. GOETZ*, YUFANG JIN‡ and JAMES T. RANDERSON‡

Woods Hole Research Center, 149 Woods Hole Rd, Falmouth, MA 02540, USA, †Department of Geography, Colgate University, Hamilton, NY 13346, USA, ‡Department of Earth System Science, University of California, Irvine, CA 92697, USA

Abstract

The snow-masking effect of vegetation exerts strong control on albedo in northern high latitude ecosystems. Large-scale changes in the distribution and stature of vegetation in this region will thus have important feedbacks to climate. The snow-albedo feedback is controlled largely by the contrast between snow-covered and snow-free albedo ($\Delta\alpha$), which influences predictions of future warming in coupled climate models, despite being poorly constrained at seasonal and century time scales. Here, we compare satellite observations and coupled climate model representations of albedo and tree cover for the boreal and Arctic region. Our analyses reveal consistent declines in albedo with increasing tree cover, occurring south of latitudinal tree line, that are poorly represented in coupled climate models. Observed relationships between albedo and tree cover differ substantially between snow-covered and snow-free periods, and among plant functional type. Tree cover in models varies widely but surprisingly does not correlate well with model albedo. Furthermore, our results demonstrate a relationship between tree cover and snow-albedo feedback that may be used to accurately constrain high latitude albedo feedbacks in coupled climate models under current and future vegetation distributions.

Keywords: albedo, arctic, boreal forest, climate feedback, CMIP5, global change, vegetation cover

Received 24 June 2013 and accepted 5 August 2013

Introduction

Northern high latitude ecosystems are experiencing amplified climate warming (Serreze & Barry, 2011) that will be exacerbated by a series of positive feedbacks (Chapin *et al*., 2005), the relative magnitudes of which remain uncertain. A terrestrial albedo feedback to climate is underway in these ecosystems and being driven by two processes: densification and northward expansion of woody vegetation (Thompson *et al*., 2004; Beringer *et al*., 2005; Pearson *et al*., 2013) and changes in the extent and duration of snow cover (Chapin *et al*., 2005; Déry & Brown, 2007). Currently, snow melt advance exerts the strongest feedback on regional warming (Chapin *et al*., 2005), however, continued increases in tree and shrub cover will likely diminish its role (Chapin *et al*., 2005; Matthes *et al*., 2011). Amplified regional warming as a consequence of the albedo feedback (Chapin *et al*., 2005) is expected to accelerate permafrost thaw (Bonfils *et al*., 2012) which will mobilize previously inaccessible soil carbon pools (Schuur *et al*., 2009). Conversely, cooling as a consequence of deforestation or fire disturbance has been observed at local scales (Lee *et al*., 2011) as well as in regional model experiments (Betts, 2000; Bathiany *et al*., 2010; Rogers *et al*., 2013). Therefore, widespread changes in the stature and distribution of vegetation stand to play an important role in determining the magnitude and timing of further regional and global climate warming (Chapin *et al*., 2005).

The decline in albedo ($\Delta\alpha$) between snow-covered and snow-free conditions represents the strength of the albedo feedback associated with changes in the length of the snow-free growing season (Qu & Hall, 2007; Fernandes *et al*., 2009). In climate models, this snow-albedo-feedback (SAF) can be defined as the change in albedo forced by a change in temperature (i.e. $\Delta\alpha/\Delta T$), typically calculated at decadal timescales and large spatial scales (e.g. poleward of 30°N latitude). SAF is a known source of uncertainty in estimates of 21st century warming among climate models (Hall & Qu, 2006; Fletcher *et al*., 2012). Variability in SAF is particularly pronounced in the boreal region (Qu & Hall, 2013) and has been attributed to variability in $\Delta\alpha$, partly resulting from differences in how models treat the snow-masking effects of vegetation (Qu & Hall, 2007, 2013). As the vertical stature of vegetation increases, $\Delta\alpha$ decreases (Sturm *et al*., 2005; Loranty *et al*., 2011), effectively

Correspondence: Michael M, Loranty, tel. 315-228-6057, fax 315-228-7038, e-mail: mloranty@colgate.edu

reducing the strength of SAF and diminishing the role of increased snow-free season length on the overall albedo feedback (Chapin *et al*., 2005). To estimate the impacts of albedo changes on continued regional warming a comprehensive quantitative understanding of the relationship between vegetation structure and SAF strength is necessary.

Northward migration of boreal tree line has long been recognized as a potentially important climate feedback (Bonan *et al*., 1992). However, much recent research has emphasized the impacts of shrub expansion in tundra ecosystems (Sturm *et al*., 2001; Chapin *et al*., 2005; Elmendorf *et al*., 2012) on surface energy budgets (Sturm *et al*., 2005). This is primarily due to widespread shrub cover (Beck *et al*., 2011b) with expansion relying less on dispersal and colonization and therefore occurring more rapidly (Sturm *et al*., 2001; Tape *et al*., 2006; Forbes *et al*., 2010) than tree line advance (e.g. <1 km per decade; Chapin *et al*., 2005). Efforts have been made to include more detailed representation of high latitude vegetation in coupled climate models for the purpose of quantifying the magnitude of regional albedo feedbacks, as well as their impacts on permafrost dynamics (Lawrence & Swenson, 2011; Bonfils *et al*., 2012). However, the focus on tundra vegetation implicitly assumes that boreal forest delineation, vegetation distribution, and albedo are accurately characterized in models, and further, that changes in albedo as a consequence of shifts in vegetation distribution are less likely in boreal forests. Here, we test the assumption of accurate spatial characterization of boreal forest canopy biophysical properties in models by comparing satellite observations of vegetation cover and albedo with data from coupled climate models archived as part of the Coupled Model Intercomparison Project Phase 5 (CMIP5; Taylor *et al*., 2012).

Materials and methods

Satellite data

Shortwave (0.3–5.0 μm) broadband albedo data were generated using the Moderate Resolution Imaging Spectroradiometer (MODIS) MCD43B3 1 km spatial resolution standard product (Schaaf *et al*., 2002). Data were screened to include only high quality full Bidirectional Reflectance Distribution Function inversions with solar zenith angles less than 70°. Proportions of direct and diffuse radiation were computed using zenith angle at local solar noon and an assumed aerosol optical depth of 0.2 (O'Halloran *et al*., 2012) with code provided by the MODIS albedo science team (www.modis.bu.edu/brdf/userguide/tools.html). Monthly values for April and July were calculated by taking the mean of all composites with at least 80% (13 of 16 days) occurring during each month for the 2006–2010 period. For percent tree cover we used a version of the Collection 4 MODIS Vegetation Continuous Fields (VCF; Hansen *et al*., 2003) product modified to improve representation of circumpolar tree line (Ranson *et al*., 2011), augmented with data from the Collection 5 VCF product

Table 1 Earth system models from the Coupled Model Intercomparison Project 5 (CMIP5)

			Spatial Resolution	
Modeling Group	No.	Model	Lat	Lon
Commonwealth Scientific and Industrial Research Organization (CSIRO) and Bureau of Meteorology (BOM), Australia	1	ACCESS1.0	1.25°	1.875°
	2	ACCESS1.3	1.25°	1.875°
Beijing Normal University, College of Global Change and Earth System Science	3	BNU-ESM	2.79°	2.81°
NOAA, Geophysical Fluid Dynamics Laboratory	4	GFDL-ESM2M	2.50°	2.01°
The Met Office Hadley Centre	5	HadGEM2-CC	1.88°	1.25°
	6	HadGEM2-ES	1.88°	1.25°
Russian Academy of Sciences, Institute of Numerical Mathematics	7	INM-CM4	2.00°	1.50°
Institute Pierre-Simon Laplace	8	IPSL-CM5A-LR	3.75°	1.89°
Japan Agency for Marine-Earth Science and Technology, Atmosphere and Ocean Research Institute (The University of Tokyo), National Institute for Environmental Studies	9	MIROC-ESM	2.81°	2.79°
	10	MIROC5	1.41°	1.40°
Max Plank Institute for Meteorology	11	MPI-ESM-LR	1.88°	1.86°

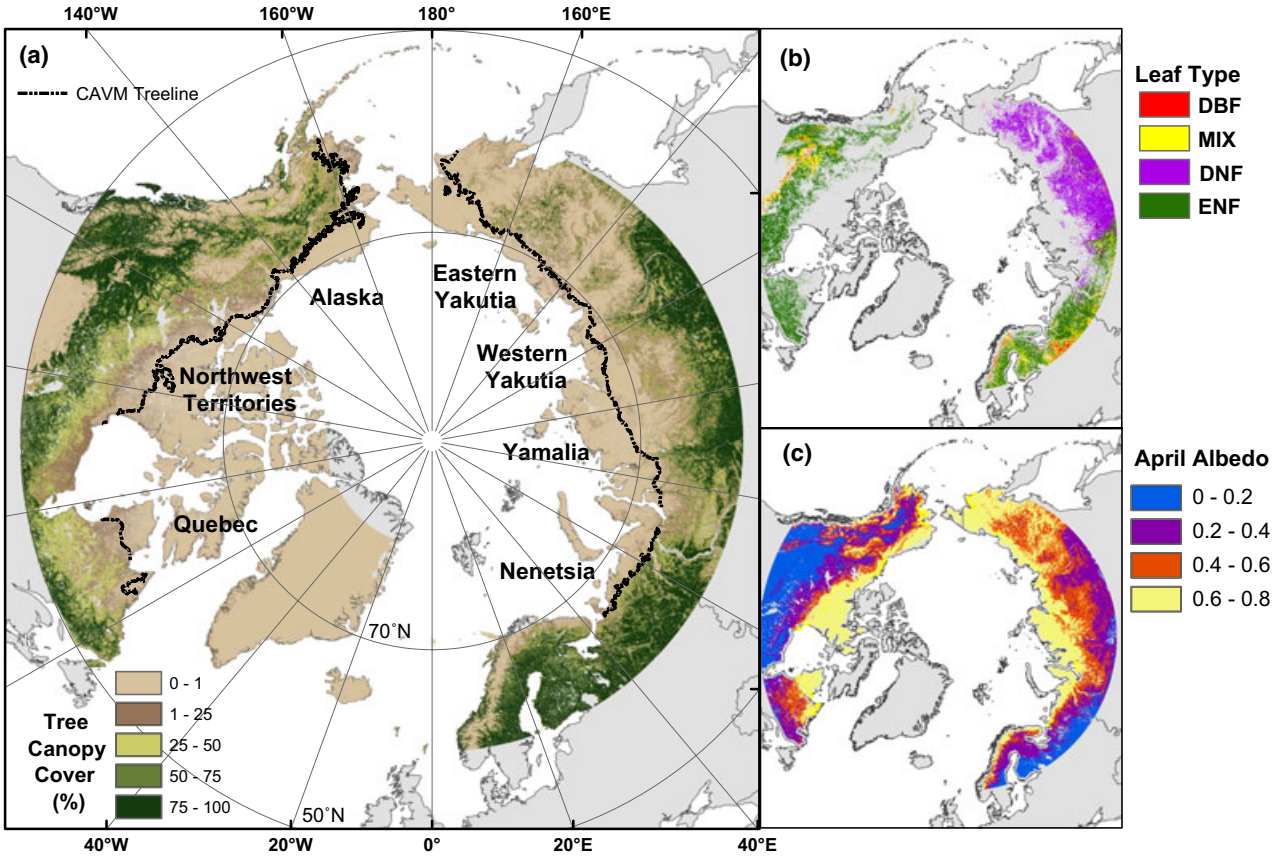

Fig. 1 Map of the study domain showing variability in MODIS tree cover (main panel), GLC-2000 plant functional type for boreal forest (upper right) and MODIS albedo for April 2006–2010 (lower right). A low pass filter was applied to the albedo data to improve visual interpretation. Forest types are as follows: deciduous broadleaf forest (DBF), deciduous needleleaf forest (DNF), evergreen needleleaf forest (ENF) and mixed-leaf forest (MIX).

northward of 70°, both at 1 km spatial resolution. We also used the United States Geological Survey's GTOPO30 elevation data set, and tree line delineated as part of the Circumpolar Arctic Vegetation Map (CAVM; Walker *et al.*, 2005).

Climate model data

CMIP5 data were downloaded from the Earth System Grid (http://pcmdi3.llnl.gov/esgcet/home.htm). We acquired all models (n = 11) from the representative concentration pathway 8.5 (RCP8.5) experiment (ensemble r1i1p1) for which tree cover ('treeFrac') outputs were available in December 2012. Model albedo was calculated as the ratio of upwelling to downwelling clear sky shortwave radiation. Means of albedo, 2 m air temperature and percent tree cover from April to July for the 2006–2010 and 2095–2099 time periods were used for analyses. SAF was calculated as the quotient of the difference between April and July albedo ($\Delta\alpha$) and the difference between mean April and July 2 m air temperature (ΔT);

$$\mathrm{SAF} = \frac{\alpha_{\mathrm{April}} - \alpha_{\mathrm{July}}}{T_{\mathrm{April}} - T_{\mathrm{July}}} = \frac{\Delta\alpha}{\Delta T} \quad (1)$$

Using this equation we calculated SAF for each model under current (2006–2010) and future (2095–2099) conditions.

Geospatial analysis

We combined tree cover and albedo data from MODIS and the CMIP5 (Table 1) models with land cover data from the GLC2000 and the CAVM tree line map to investigate changes in surface biophysics in the circumpolar forest-tundra transition zone (Brovkin *et al.*, 2013). The spatial extent of the study domain ranged from 50° to 80° North in North America and from 60° to 80° North in Eurasia, the southern edge of which was defined by the extent of the modified MODIS tree cover data. We transformed all raster data sets to the Polar Lambert Azimuthal Equal-Area projection prior to analysis. Maps for showing the distance of each pixel to CAVM tree line were created at the resolution of each data product (e.g. MODIS albedo and VCF, and each CMIP5 model). Using the map of distance to tree line we then summarized the biophysical parameters (median, second and fourth quantiles) at each distance step across both the entire study domain and seven regional latitudinal transects that were 200 km wide and 1600 km long. At each distance step from tree line we also cal-

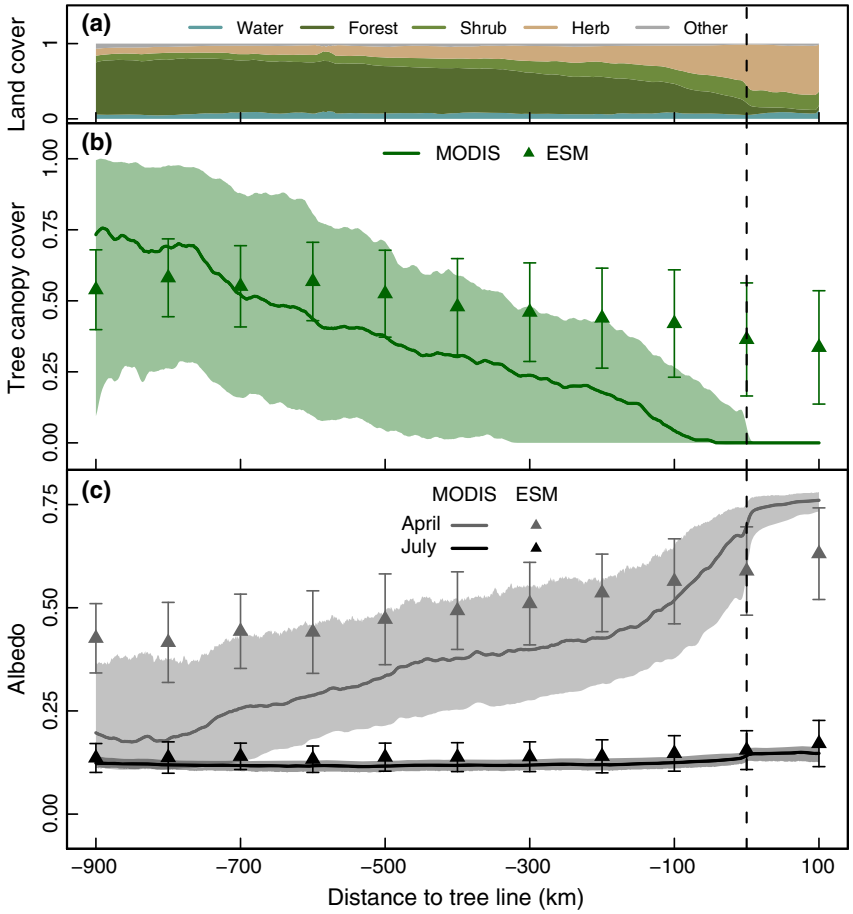

Fig. 2 Land cover type as a function of distance to tree line, as defined by the Circumpolar Arctic Vegetation Map (CAVM: a). The middle panel (b) shows decreasing proportion of forest canopy cover occurring well south of tree line. Bottom panel (c) shows decreasing April and July MODIS albedo south of treeline. Solid lines with shaded bands represent means and interquartile ranges of MODIS observations, respectively. Triangles and whiskers represent multimodel means and interquartile ranges, respectively, for tree cover (middle) and albedo (bottom).

culated the proportion of the landscape that was water, forest, shrub, herb, or some other land cover type, as defined by the GLC2000. Mean tree cover and albedo were then calculated for each CMIP5 model at 100 km intervals. The model averages at each distance interval were then averaged across all models.

Relationships between MODIS albedo and tree cover were characterized by calculating summary statistics of albedo binned at intervals of 1% tree cover. For CMIP5 models relationships between tree cover and albedo were binned at intervals of 10% tree cover using both CMIP5 tree cover and MODIS VCF resampled to model resolution. Relationships between albedo and tree cover variables were assessed using nonlinear regressions. Relationships between MODIS and CMIP5 variables were evaluated using coefficients od determination (r^2), and Wilcoxon Rank Sum tests performed in R (R Development Core Team, 2012). To compare tree cover and albedo from MODIS and the CMIP5 models we aggregated MODIS observations to match the lower spatial resolution of each model. Areas with insufficient MODIS observations (data coverage <75%) at model resolution were excluded from the analysis, as were areas within 50 km of the coast. The GLC2000 land cover data set (Bartholomé & Belward, 2005) was used to stratify the study area by PFT. For CMIP5 data sets GLC2000 was resampled to model resolution and a threshold of 50% was used to assign PFT. Grid cells where no single PFT exceeded 50% but the sum needleleaf and deciduous exceeded 50% were assigned to the mixed forest PFT. We used Pearson's correlations to evaluate the associations between MODIS and each CMIP5 model for tree cover, April albedo and July albedo across the study domain and within PFT.

Results

Satellite observations capture a gradual increase in tree cover south of latitudinal tree line (Fig. 1), accompanied by a gradual decrease in albedo (from ~0.75 to around 0.25) in April (snow-covered) but not July (snow-free) due to the snow-masking effects of vegetation. The biophysical gradient across latitudinal

Table 2 Mean values of tree cover, April albedo and July albedo over the study domain. CMIP5 data are reported model variables, MODIS data represent satellite observations scaled to the resolution of each model. Boreal data are averaged over the entire study area, data for different plant functional types are reported as well. Values in parentheses represent one SD of the mean

			Tree Cover			April Albedo			July Albedo		
	Model resolution	n*	CMIP5	MODIS	r^2†	CMIP5	MODIS	r^2	CMIP5	MODIS	r^2
Boreal	ACCESS1.0	1328	30.3 (26.1)¶	35.9 (30.1)	0.64	0.49 (0.19)¶	0.43 (0.22)	0.68	0.11 (0.02)¶	0.12 (0.02)	0.04
	ACCESS1.3	1328	36.9 (35.0)¶	35.9 (30.1)	0.81	0.42 (0.17)¶	0.43 (0.22)	0.65	0.08 (0.02)¶	0.12 (0.02)	0.04
	BNU	422	0.1 (0.2)¶	37.2(28.0)	0.04	0.58 (0.12)¶	0.44 (0.22)	0.20	0.09 (0.04)¶	0.12 (0.02)	ns
	GFDL	690	91.2 (14.9)¶	36.2(29.2)	ns	0.39 (0.08)¶	0.44 (0.23)	0.12	0.15 (0.02)¶	0.12 (0.03)	0.21
	HadGEM2CC	1328	18.5 (31.7)¶	35.9 (30.1)	0.29	0.48 (0.18)¶	0.43 (0.22)	0.49	0.10 (0.03)¶	0.12 (0.02)	0.03
	HadGEM2ES	1328	23.2 (35.0)¶	35.9 (30.1)	0.32	0.43 (0.18)	0.43 (0.22)	0.48	0.10 (0.03)¶	0.12 (0.02)	0.03
	INMCM4	1062	13.6 (13.8)¶	35.8 (29.7)	0.32	0.54 (0.18)¶	0.43 (0.23)	0.54	0.20 (0.06)¶	0.12 (0.02)	0.14
	IPSL	449	53.4 (26.5)¶	35.6 (28.8)	0.62	0.37 (0.13)¶	0.44 (0.23)	0.67	0.19 (0.02)¶	0.12 (0.02)	0.08
	MIROCESM	422	54.9 (32.7)¶	37.2 (28.0)	0.25	0.61 (0.16)¶	0.44 (0.22)	0.35	0.13 (0.03)§	0.12 (0.02)	0.07
	MIROC5	1294	96.9 (8.3)¶	36.2 (30.0)	0.01	0.58 (0.19)¶	0.43 (0.22)	0.64	0.12 (0.03)¶	0.12 (0.02)	0.11
	MPI	972	28.3 (21.6)¶	35.8 (29.3)	0.46	0.46 (0.21)¶	0.43 (0.23)	0.57	0.16 (0.03)¶	0.12 (0.02)	0.14
	Mean		**40.7 (30.9)**	**36.1 (0.5)**	**0.38**	**0.49 (0.08)**	**0.43 (0.01)**	**0.49**	**0.13 (0.04)**	**0.12 (0.00)**	**0.09**
Evergreen needleleaf	ACCESS1.0	249	53.9 (18.2)¶	63.7 (19.5)	0.37	0.32 (0.13)¶	0.23 (0.11)	0.47	0.11 (0.01)¶	0.10 (0.02)	ns
	ACCESS1.3	249	74.7 (22.2)¶	63.7 (19.5)	0.52	0.26 (0.12)¶	0.23 (0.11)	0.53	0.07(0.00)¶	0.10 (0.02)	ns
	BNU	65	0.1 (0.2)¶	63.1 (19.1)	ns	0.51 (0.13)¶	0.22 (0.10)	0.07	0.08 (0.02)¶	0.11 (0.02)	0.09
	GFDL	121	89.7 (14.5)¶	64.8 (19.7)	0.02	0.39 (0.08)¶	0.22 (0.12)	0.11	0.15 (0.01)¶	0.10 (0.02)	ns
	HadGEM2CC	249	45.9 (34.7)¶	63.7 (19.5)	0.09	0.30 (0.11)¶	0.23 (0.11)	0.20	0.10 (0.01)¶	0.10 (0.02)	0.03
	HadGEM2ES	249	59.0 (32.8)	63.7 (19.5)	0.05	0.25 (0.10)	0.23 (0.11)	0.11	0.10 (0.01)¶	0.10 (0.02)	0.03
	INMCM4	203	28.6 (10.7)¶	65.1 (19.1)	0.06	0.39 (0.16)¶	0.22 (0.12)	0.42	0.16 (0.01)¶	0.10 (0.02)	0.02
	IPSL	79	79.8 (16.7)¶	62.2 (19.8)	0.24	0.26 (0.08)¶	0.23 (0.12)	0.35	0.17 (0.01)¶	0.10 (0.02)	0.10
	MIROCESM	65	73.5 (16.6)§	63.1 (19.1)	0.04	0.49 (0.11)¶	0.22 (0.10)	0.09	0.11 (0.00)	0.11 (0.02)	0.19
	MIROC5	291	97.2 (5.5)¶	64.4 (19.6)	0.02	0.41 (0.14)¶	0.23 (0.12)	0.53	0.10 (0.00)¶	0.11 (0.02)	ns
	MPI	168	44.1 (14.4)¶	62.5 (19.8)	0.08	0.28 (0.14)¶	0.22 (0.11)	0.10	0.14 (0.01)¶	0.10 (0.02)	0.06
	Mean		**58.8 (28.5)**	**63.6 (0.9)**	**0.15**	**0.35 (0.09)**	**0.23 (0.01)**	**0.27**	**0.12 (0.03)**	**0.10 (0.00)**	**0.07**
Deciduous needleleaf	ACCESS1.0	196	47.3 (20.7)¶	42.4 (29.2)	0.35	0.49 (0.10)¶	0.41 (0.11)	0.34	0.11 (0.01)¶	0.12 (0.01)	0.09
	ACCESS1.3	196	40.1 (32.2)¶	42.4 (29.2)	0.90	0.46 (0.10)¶	0.41 (0.11)	0.19	0.07 (0.00)¶	0.12 (0.01)	ns
	BNU	52	0.1 (0.1)¶	44.3 (27.6)	ns	0.63 (0.01)¶	0.43 (0.11)	ns	0.08 (0.01)¶	0.12 (0.01)	ns
	GFDL	93	98.0 (2.6)¶	44.0 (28.7)	ns	0.37 (0.06)¶	0.42 (0.12)	0.09	0.15 (0.00)¶	0.12 (0.01)	0.06
	HadGEM2CC	196	0.0 (0.0)¶	42.4 (29.2)	ns	0.60 (0.04)¶	0.41 (0.11)	0.26	0.10 (0.00)¶	0.12 (0.01)	ns
	HadGEM2ES	196	0.0 (0.0)¶	42.4 (29.2)	ns	0.56 (0.04)¶	0.41 (0.11)	0.31	0.10 (0.00)¶	0.12 (0.01)	ns
	INMCM4	146	3.8 (4.9)¶	43.7 (28.8)	0.35	0.67 (0.04)¶	0.42 (0.12)	0.34	0.19 (0.02)¶	0.12 (0.01)	ns
	IPSL	60	63.9 (24.8)¶	43.0 (29.1)	0.63	0.36 (0.10)¶	0.42 (0.11)	0.25	0.18 (0.02)¶	0.12 (0.01)	ns
	MIROCESM	52	55.5 (33.2)¶	44.3 (27.6)	0.34	0.76 (0.04)¶	0.43 (0.11)	0.04	0.12 (0.02)	0.12 (0.01)	0.05
	MIROC5	224	99.7 (1.5)¶	43.9 (29.2)	ns	0.63 (0.11)¶	0.42 (0.11)	0.30	0.11 (0.02)¶	0.12 (0.01)	ns
	MPI	138	31.1 (19.2)¶	44.4 (29.2)	0.77	0.54 (0.12)¶	0.41 (0.12)	0.33	0.16 (0.01)¶	0.12 (0.01)	ns
	Mean		**40.0 (37.4)**	**43.4 (0.9)**	**0.56**	**0.55 (0.12)**	**0.42 (0.01)**	**0.25**	**0.12 (0.04)**	**0.12 (0.00)**	**0.07**

Table 2 (continued)

	Model resolution	n*	Tree Cover			April Albedo			July Albedo		
			CMIP5	MODIS	r^2†	CMIP5	MODIS	r^2	CMIP5	MODIS	r^2
Mixed	ACCESS1.0	61	50.2 (23.6)¶	70.1 (17.9)	0.37	0.36 (0.18)¶	0.25 (0.14)	0.55	0.12 (0.01)	0.12 (0.01)	ns
	ACCESS1.3	61	70.7 (32.6)§	70.1 (17.9)	0.52	0.27 (0.18)¶	0.25 (0.14)	0.63	0.07 (0.00)¶	0.12 (0.01)	ns
	BNU	16	0.0 (0.1)¶	57.2 (20.4)	ns	0.60 (0.07)§	0.31 (0.16)	ns	0.08 (0.01)¶	0.11 (0.02)	ns
	GFDL	40	92.0 (12.7)¶	58.6 (23.2)	ns	0.40 (0.06)¶	0.29 (0.16)	0.44	0.15 (0.01)¶	0.12 (0.02)	ns
	HadGEM2CC	61	43.2 (41.4)¶	70.1 (17.9)	0.42	0.32 (0.18)¶	0.25 (0.14)	0.59	0.10 (0.01)¶	0.12 (0.01)	ns
	HadGEM2ES	61	50.4 (41.4)¶	70.1 (17.9)	0.39	0.29 (0.16)¶	0.25 (0.14)	0.56	0.10 (0.01)¶	0.12 (0.01)	ns
	INMCM4	52	17.8 (12.7)¶	55.8 (25.2)	0.13	0.53 (0.18)¶	0.32 (0.20)	0.51	0.18 (0.03)¶	0.12 (0.02)	ns
	IPSL	22	70.5 (21.4)	68.9 (13.5)	ns	0.30 (0.10)‡	0.27 (0.12)	0.29	0.17 (0.02)¶	0.12 (0.02)	ns
	MIROCESM	16	75.3 (12.6)¶	57.2 (20.4)	0.18	0.52 (0.13)§	0.31 (0.16)	0.26	0.12 (0.01)	0.11 (0.02)	ns
	MIROC5	70	98.7 (2.8)¶	62.7 (19.2)	ns	0.47 (0.17)¶	0.30 (0.17)	0.66	0.10 (0.01)¶	0.12 (0.02)	ns
	MPI	51	46.4 (21.7)¶	59.0 (25.6)	0.19	0.36 (0.19)¶	0.29 (0.19)	0.60	0.14 (0.02)¶	0.12 (0.02)	ns
	Mean		**55.9 (29.7)**	**63.6 (6.2)**	**0.31**	**0.40 (0.11)**	**0.28 (0.03)**	**0.51**	**0.12 (0.04)**	**0.12 (0.00)**	

*Number of pixels with for each model (Boreal) and occupied by at least 50% of the relevant pant functional type (e.g. evergreen needleleaf, etc.…).
†r^2 values represent Pearson correlation coefficients between CMIP5 data and MODIS observations scaled to model resolution.
‡Means significantly different at $P < 0.1$ using Wilcoxon Rank Sum test.
§Means significantly different at $P < 0.05$ using Wilcoxon Rank Sum test.
¶Means significantly different at $P < 0.01$ using Wilcoxon Rank Sum test.
Values in bold type indicate multi-model means.

Fig. 3 Observed seasonal albedo change (April–July) as a functions MODIS tree cover (left column) and CMIP5 model tree cover (right column). The top panel shows data for the entire study domain, and the following panels are for the areas dominated by evergreen needleleaf forests (ENF), deciduous needleleaf forests (DNF) and broadleaf-conifer mixed forests (MIX) as identified by GLC2000. MODIS data represent means (black lines) and interquartile ranges (gray shading) for albedo binned by increments of 1% tree cover. CMIP5 data are binned to nearest 10% tree cover for clarity. The multimodel mean represents the average (black line) and interquartile range (gray shading) of each 10% tree cover bin

tree line exhibits considerable geographic variability (Fig. 1, Figs S2–9). Regional differences in the magnitude of snow-covered and snow-free albedo (e.g. Fig. S3 vs. S5) correspond to differences in PFT (Fig. 1). Abrupt biophysical transitions that are consistent with cartographic representations of tree line are often apparently associated with topographic barriers (e.g. Fig. S9). Elsewhere the biophysical transition associated with latitudinal tree line occurs gradually over distances of 50–400 km and varies with differences in fractional tree cover (Figs S3–S8).

Multimodel means for the eleven CMIP5 models (Table 1) show much smaller latitudinal changes in both tree cover and albedo than the MODIS products (Fig. 2). Significant biases are evident in tree cover and April albedo. Differences in tree cover between models and satellite observations decrease moving southward from tree line (Fig. 2b), while albedo differences increase (Fig. 2c). These general patterns were also apparent when the CMIP5 models were individually compared with MODIS (Fig. S1).

We resampled MODIS observations to the resolution of each CMIP5 model to account for uncertainties related to spatial aggregation when comparing the two data sets (Table 2). Mean CMIP5 tree cover of $40.6 \pm 30.9\%$ is greater and more variable than the mean aggregate MODIS tree cover of $36.1 \pm 0.5\%$ ($\pm$SD). Average CMIP5 albedo for April and July were 0.49 ± 0.08 and 0.13 ± 0.04, respectively, which were also biased high in relation with the MODIS means of 0.43 ± 0.005 for April and 0.12 ± 0.006 for July. Mean tree cover and albedo varied widely between models, as evidenced by the high standard deviation and differences between CMIP5 models and MODIS over the entire study region, as well as within plant functional types (Table 2). These differences in mean tree cover and albedo were significant in nearly all cases ($P < 0.1$–0.01, Wilcoxon Rank Sum test; Table 2). The Hadley Centre ESM accounted for most of the exceptions, showing good agreement with April albedo, as well as tree cover in areas dominated by evergreen needleleaf vegetation. Pearson's correlation coefficients showed highest agreement between CMIP5 models and MODIS for April albedo (mean $r^2 = 0.49 \pm 0.19$; Table 2), followed by tree cover ($r^2 = 0.38 \pm 0.26$), indicating models captured spatial patterns of April albedo, and in some cases tree cover, reasonably well. Correlations between CMIP5 and MODIS July albedo were weak owing to the relative homogeneity of albedo under snow-free conditions (Table 2).

There were mostly nonlinear relationships between satellite observations of $\Delta\alpha$ (April–July) and tree cover (Fig. 3, Table S1) and, when evaluated with MODIS tree cover, model $\Delta\alpha$ corresponded to the observed relationship reasonably well. Among PFTs, model averages of $\Delta\alpha$ show the best agreement with observations in areas dominated by evergreen needleleaf forest (Fig. 3b, Table 2, Table S1), and tend towards a high bias in areas dominated by mixed forests and deciduous needleleaf forests (Fig. 3c and d, Table 2). The multimodel mean shows good agreement with the observed trends but is biased high. Correlations between model tree cover and albedo varied widely in comparison to observed relationships (Fig. 3e–h, Figs S10 and S11e–h) and correlations, when present, were generally not strong (Table 2, Table S1). Maps of differences between model and observed tree cover reveal that models which over-predicted tree cover tended to assign values of 100% tree cover to all grid cells dominated by a forest land cover type (Fig. 4). Under-predicting models tended to assign low values to sparsely forested areas near tree line and in larch forests of eastern Siberia (Fig. 4, Table 2). Although the relationships between model tree cover and $\Delta\alpha$ are variable, the CMIP5 relationship between multimodel mean tree cover and $\Delta\alpha$ agreed closely with observations (Fig. 3e–h). However, not all of the models captured tree cover equally well (Fig. 4), which means that they are not equally weighted. The multimodel mean nonlinear relationships between tree cover and albedo, for all time periods and PFTs, were significantly different from the corresponding relationships for MODIS observations (Fig. 2, Figs S10 and S11, Table S1).

Among models there was a strong relationship between the snow-albedo feedback and MODIS tree cover (Fig. 5a). Increased tree cover results in a decrease in the snow-albedo feedback due to the decrease in $\Delta\alpha$ (Fig. 3). The relationship between changes in model tree cover and seasonal SAF between 2010 and 2100 illustrates this point (Fig. 5b), showing more change in the seasonal SAF among models that exhibit no change in tree cover than in those that do.

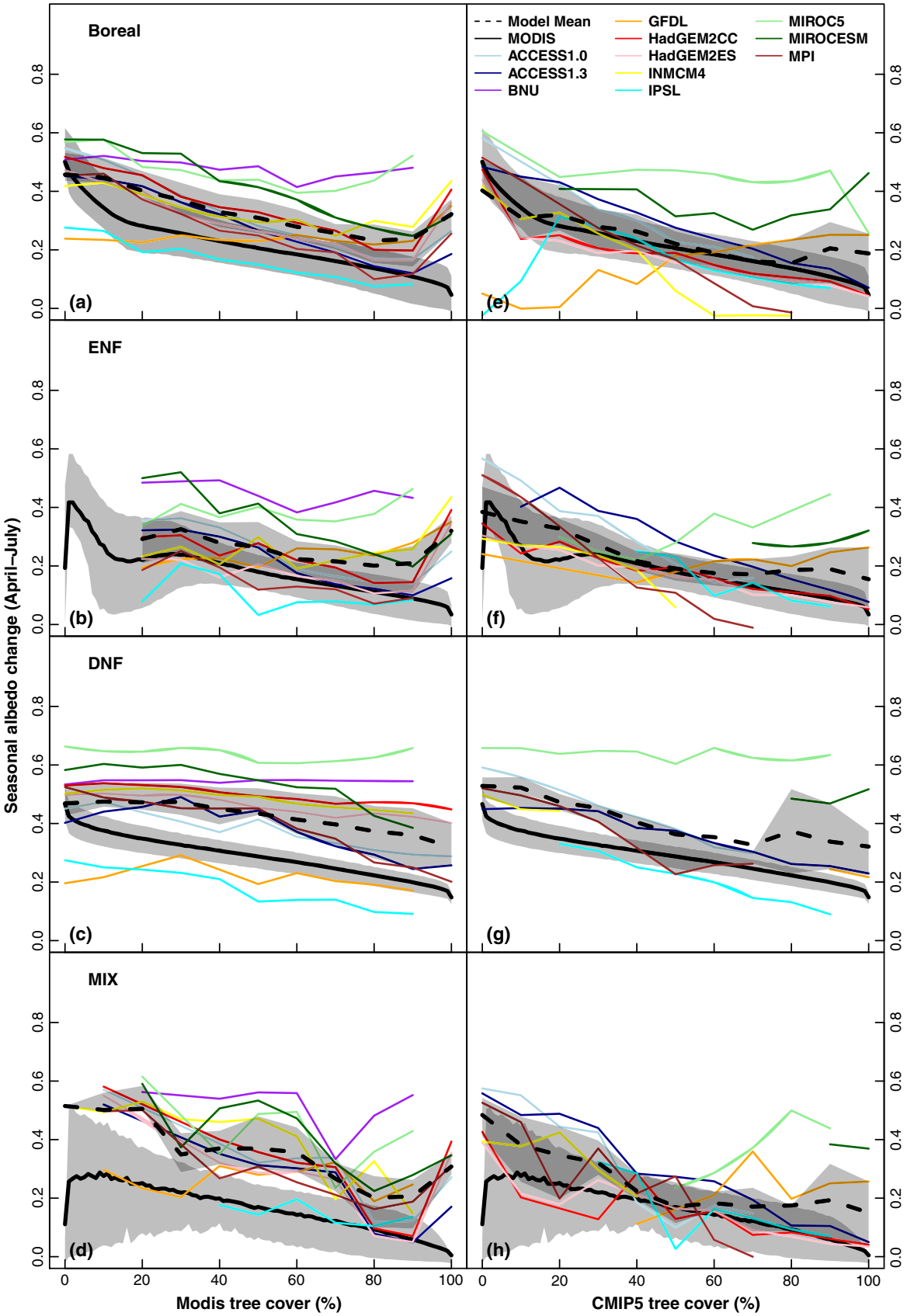
Boreal
ENF
DNF
MIX
(a)
(b)
(c)
(d)
(e)
(f)
(g)
(h)
Model Mean
MODIS
ACCESS1.0
ACCESS1.3
BNU
GFDL
HadGEM2CC
HadGEM2ES
INMCM4
IPSL
MIROC5
MIROCESM
MPI
Seasonal albedo change (April–July)
Modis tree cover (%)
CMIP5 tree cover (%)
0.0
0.2
0.4
0.6
0.8
0
20
40
60
80
100

Discussion

How does albedo vary across the pan-boreal region?

Our spatial analyses of MODIS observations revealed a gradual decline in fractional tree cover with increasing latitude (Figs 1a and b, 2a), reinforcing the idea that simple biome-wide averages do not sufficiently represent the salient biophysical characteristics of terrestrial ecosystems. The corresponding increase in albedo with latitude is most pronounced during periods of snow cover (Figs 1c and 2c). These general patterns broadly characterize the study area, however, regional differences in the magnitude of these gradients associated with topography (Fig. 2, Figs S2–S9) and PFT (Figs 2b and c, 3a–d) highlight the importance of characterizing structural heterogeneity within regions characterized by similar ecosystem types. Differences in PFT also contributed to substantial variability in albedo across the pan-boreal study region (Figs 2b, c and 3a–d), particularly during periods of snow cover (Fig. 2c, Fig. S10). While the influence of canopy cover and PFT on albedo may seem intuitive, our results illustrate a high degree of variability within the boreal biome and highlight the possibility of processes such as disturbance (Jin *et al.*, 2012a,b) and forest infilling (Wilmking *et al.*, 2006; Mamet & Kershaw, 2011) to exert strong influence on high northern latitude albedo dynamics. Perhaps more importantly, these processes will be heterogeneous in space and time due to biological differences in dominant tree species such as serotiny in evergreen needleleaf species (e.g. *Picea mariana*) or clonal reproduction in broadleaf deciduous species (e.g. *Populus tremuloides*), and differential responses of PFTs to spatially variable environmental drivers and disturbance (e.g. Ewers *et al.*, 2005).

Representation of boreal land-surface biophysics in climate models

Average climate model representations of latitudinal gradients did not generally match observations (Fig. 1). Differences in latitudinal tree cover and albedo gradients may be partially explained by the relatively coarse resolution of CMIP5 models relative to MODIS, particularly in regional examples that include very few grid cells (Figs S2–S9). Models with higher spatial resolution or that employ tiling within grid cells are in theory better able to represent spatial gradients in vegetation cover.

On average CMIP5 $\Delta\alpha$ was well correlated with MODIS tree cover (Fig. 3a–d), indicating models reasonably captured spatial variability in albedo, particularly as it relates to variability in tree cover. This is not unexpected given the strong agreement between MODIS and CMIP5 April albedo (Table S1). Relationships between multimodel mean $\Delta\alpha$ and MODIS tree cover were biased high relative to observational relationships. The factors contributing to bias in $\Delta\alpha$ differ between models but include errors associated with PFT and seasonal albedo (Figs S10 and S11). For example, the IPSL model reasonably approximates April albedo (Fig. S10), but over-predicts July albedo (Fig. S11) for all PFTs, resulting in a value of $\Delta\alpha$ that is biased low (Fig. 3). Conversely, the MIROC-ESM model reasonably captures July albedo, but over-predicts April albedo leading to values of $\Delta\alpha$ that are biased high (Fig. 3a–d). More generally, models showed best agreement with observed relationships for grid cells dominated by evergreen needleleaf forests (Fig. 3b), indicating that models rely heavily on biophysical characteristics of evergreen needleleaf forests, or perhaps that deciduous needleleaf and mixed forests are poorly characterized despite their being widespread across the boreal biome (Fig. 1).

Relationships between CMIP5 $\Delta\alpha$ and CMIP5 tree cover (Fig. 3e–h), where present, were not as strong and highly variable in comparison with the relationship between CMIP5 $\Delta\alpha$ and MODIS tree cover (Fig. 3a–d). This is due to variability in model representations of tree cover (Fig. 4), with some models exhibiting an apparent disconnect between tree cover and albedo due to overly generalized characterizations of forest distribution (e.g. GFDL and MIROC5) while others have strong relationships between these two variables owing to more detailed spatial representations of boreal forest PFTs (e.g. Had, IPSL and MPI). Overly general characterizations of forest cover may be problematic even in models without dynamic vegetation, depending on how model albedo is calculated during periods of snow cover.

Albedo calculations in climate models may be relatively complex and utilize radiative transfer schemes in conjunction with areal snow cover data and ground and snow albedos, or they may be as simple as weighted means of snow-free land albedo and snow albedo, where snow albedo is not dependent upon vegetation type. Schemes of intermediate complexity exist as well (Qu & Hall, 2007). Diagnosing the influence of vegetation parameterizations on albedo for all models is difficult because snow cover can influence albedo via physical characteristics such as water content and age of snowpack (Flanner & Zender, 2006), as well as its areal extent. Analyzing these physical properties is beyond the scope of our study but our results should be useful for diagnosing and refining individual models. For example, for the pan-boreal study region the ACCESS1.0 model generally agrees well with snow-free

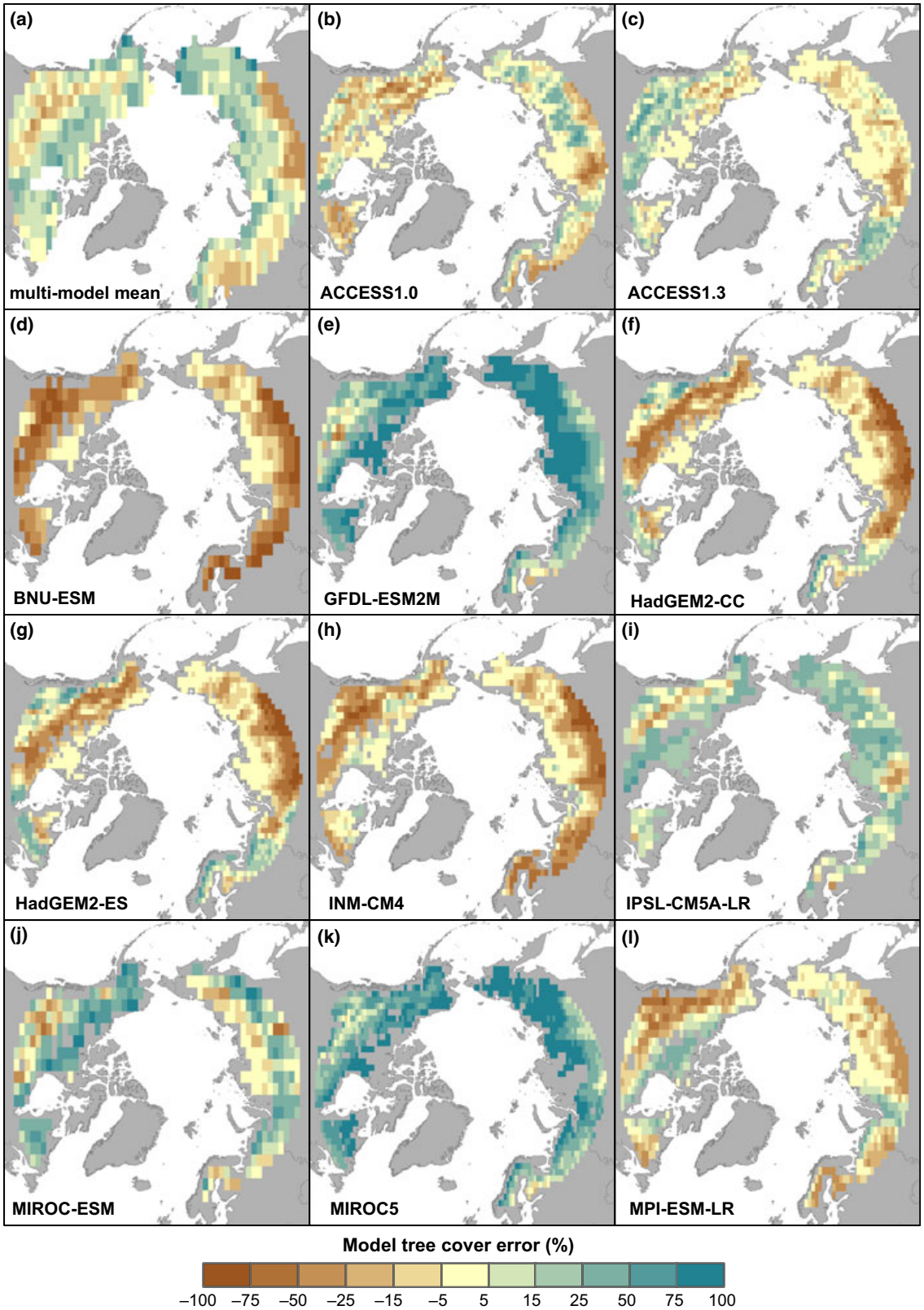

Fig. 4 Maps showing the difference between MODIS and CMIP5 (2006–2010) tree cover for the multi-model mean (a) and each model included in the analysis (b–l). MODIS tree cover data were aggregated to the resolution of each model to calculate differences. Gray areas were not included in the study domain.

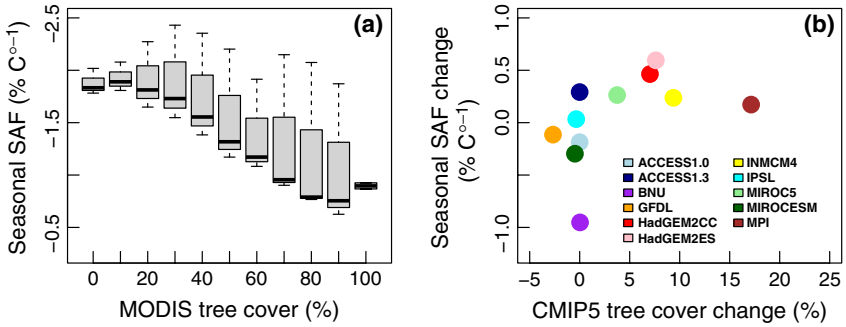

Fig. 5 Multimodel mean seasonal snow-albedo feedback (SAF) aggregated by MODIS tree cover scaled to model resolution (a). The boxplot (a) shows median (black line), interquartile range (gray shading) and extreme values (whiskers) of seasonal SAF for all 11 models. Seasonal SAF was calculated for each grid cell, and then binned to the nearest 10% tree cover. Change in seasonal SAF from 2010 to 2100 (e.g. 2095–2099 SAF – 2006–2010 SAF) as a function of change in CMIP5 tree cover over the same time period (b).

(July) albedo, but under predicts tree cover and over predicts snow-covered (April) albedo, suggesting vegetation cover is at least partially responsible for model differences from observed albedo (Table S1). On the other hand, models with apparently less sophisticated vegetation representations, such as GFDL or MIROC5, are more difficult to diagnose because snow-free albedos may agree reasonably well with observations but this outcome is difficult to discern relative to how vegetation influences albedo.

Implications for climate change

Overall, our results indicate that satellite observations are been useful to effectively inform spatial variability in land surface biophysical properties in CMIP5 models, particularly during periods of snow cover, for high northern latitudes. However, biotic factors that control this variability (e.g. tree cover) are, on average, less well represented. Accurately characterizing relationships between vegetation and albedo is increasingly important with the inclusion of dynamic vegetation in coupled climate models. This is especially true for high northern latitudes, where we found CMIP5 SAF strength decreases with increasing tree cover (Fig. 5a), but within models changes in SAF from 2010 to 2100 did not correlate well with changes in model tree cover (Fig. 5b). While other climatological factors such as precipitation may contribute to this finding (Brutel-Vuilmet *et al.*, 2013), our results illustrate the importance of vegetation influences on SAF strength. It is worth noting the importance of vegetation dynamics, as they relate to surface biophysical properties in climate models, is not restricted to high northern latitude ecosystems; anthropogenic induced changes in PFT such as tropical deforestation may occur more rapidly than high latitude vegetation change. Indeed, a similar approach to that we employed here has recently been used to assess the MPI model albedo dynamics at the global scale (Brovkin *et al.*, 2013) and satellite observations of canopy dynamics are used to assess terrestrial biogeochemical processes as well (Randerson *et al.*, 2009).

The close relationship between satellite observations of tree cover and albedo (Fig. 3a–d) indicates that information on the geographic distribution and abundance of PFT can be used to constrain albedo dynamics and SAF in coupled climate model simulations, particularly those that include dynamic vegetation. Accurate characterization of high latitude albedo dynamics is important given the potential for albedo feedbacks to amplify (Chapin *et al.*, 2005; Lawrence & Swenson, 2011; Bonfils *et al.*, 2012) or ameliorate (Betts, 2000; Lee *et al.*, 2011; Rogers *et al.*, 2013) regional warming, and consequently influence the permafrost carbon climate feedback (Lawrence & Swenson, 2011; Bonfils *et al.*, 2012). Our observations of biophysical transitions within the boreal biome suggest that processes such as forest infilling (Wilmking *et al.*, 2006; Mamet & Kershaw, 2011), disturbance (Jin *et al.*, 2012a,b) and associated changes in stature (Gamache & Payette, 2004; Macias-Fauria *et al.*, 2012) that occur more rapidly than tree line advance (Mamet & Kershaw, 2011) have the potential to result in regionally significant albedo changes in coming decades. In this regard, disturbance mediated changes in PFT (Barrett *et al.*, 2011; Beck *et al.*, 2011a; Alexander *et al.*, 2012a; Jin *et al.*, 2012a) and stand density (Alexander *et al.*, 2012b; Berner *et al.*, 2012) may be particularly important as warmer temperatures at high latitudes intensify the fire regime (Turetsky *et al.*, 2010; Kelly *et al.*, 2013). Observationally based relationships between vegetation and albedo derived from satellite data provide a relatively simple and effective approach for reducing uncertainties in coupled climate model projections.

Acknowledgements

We acknowledge support from NASA Ecosystems and Carbon Cycle Grant NNX08AG13G to SJG and JTR and NOAA Global Carbon Cycle Grant NA080AR4310526 to SJG. MML acknowledges support from the Colgate University Research Council. The authors declare no conflict of interest.

References

Alexander HD, Mack MC, Goetz S, Beck PSA, Belshe EF (2012a) Implications of increased deciduous cover on stand structure and aboveground carbon pools of Alaskan boreal forests. *Ecosphere*, **3**, art45.

Alexander HD, Mack MC, Goetz S *et al*. (2012b) Carbon accumulation patterns during post-fire succession in Cajander larch (Larix cajanderi) forests of Siberia. *Ecosystems*, **15**, 1065–1082, doi: 10.1007/s10021-012-9567-6.

Barrett K, Mcguire AD, Hoy EE, Kasischke ES (2011) Potential shifts in dominant forest cover in interior Alaska driven by variations in fire severity. *Ecological Applications*, **21**, 2380–2396.

Bartholomé E, Belward AS (2005) GLC2000: a new approach to global land cover mapping from Earth observation data. *International Journal of Remote Sensing*, **26**, 1959–1977.

Bathiany S, Claussen M, Brovkin V, Raddatz T, Gayler V (2010) Combined biogeophysical and biogeochemical effects of large-scale forest cover changes in the MPI earth system model. *Biogeosciences*, **7**, 1383–1399.

Beck PSA, Goetz SJ, Mack MC, Alexander HD, Jin Y, Randerson JT, Loranty MM (2011a) The impacts and implications of an intensifying fire regime on Alaskan boreal forest composition and albedo. *Global Change Biology*, **17**, 2853–2866.

Beck PSA, Horning N, Goetz SJ, Loranty MM, Tape KD (2011b) Shrub cover on the north slope of Alaska: a circa 2000 baseline map. *Arctic, Antarctic, and Alpine Research*, **43**, 355–363.

Beringer J, Chapin FS, Thompson CC, Mcguire AD (2005) Surface energy exchanges along a tundra-forest transition and feedbacks to climate. *Agricultural and Forest Meteorology*, **131**, 143–161.

Berner LT, Beck PSA, Loranty MM, Alexander HD, Mack MC, Goetz SJ (2012) Cajander larch (*Larix cajanderi*) biomass distribution, fire regime and post-fire recovery in northeastern Siberia. *Biogeosciences*, **9**, 3943–3959.

Betts RA (2000) Offset of the potential carbon sink from boreal forestation by decreases in surface albedo. *Nature*, **408**, 187–190.

Bonan G, Pollard D, Thompson SL (1992) Effects of boreal forest vegetation on global climate. *Nature*, **359**, 716–718.

Bonfils CJW, Phillips TJ, Lawrence DM, Cameron-Smith P, Riley WJ, Subin ZM (2012) On the influence of shrub height and expansion on northern high latitude climate. *Environmental Research Letters*, **7**, 015503.

Brovkin V, Boysen L, Raddatz T, Gayler V, Loew A, Claussen M (2013) Evaluation of vegetation cover and land-surface albedo in MPI-ESM CMIP5 simulations. *Journal of Advances in Modeling Earth Systems*, **5**, 1–10.

Brutel-Vuilmet C, Ménégoz M, Krinner G (2013) An analysis of present and future seasonal Northern Hemisphere land snow cover simulated by CMIP5 coupled climate models. *The Cryosphere*, **7**, 67–80.

Chapin F, Sturm M, Serreze M *et al*. (2005) Role of land-surface changes in Arctic summer warming. *Science*, **310**, 657.

Déry SJ, Brown RD (2007) Recent Northern Hemisphere snow cover extent trends and implications for the snow-albedo feedback. *Geophysical Research Letters*, **34**, L22504, doi: 10.1029/2007GL031474.

Elmendorf SC, Henry GHR, Hollister RD *et al*. (2012) Plot-scale evidence of tundra vegetation change and links to recent summer warming. *Nature Climate Change*, **2**, 1–5.

Ewers BE, Gower ST, Bond-Lamberty B, Wang C (2005) Effects of stand age and tree species on canopy transpiration and average stomatal conductance of boreal forests. *Plant Cell and Environment*, **28**, 660–678.

Fernandes R, Zhao H, Wang X, Key J, Qu X, Hall A (2009) Controls on Northern Hemisphere snow albedo feedback quantified using satellite Earth observations. *Geophysical Research Letters*, **36**, L21702, doi: 10.1029/2009GL040057.

Flanner MG, Zender CS (2006) Linking snowpack microphysics and albedo evolution. *Journal of Geophysical Research*, **111**, D12208.

Fletcher CG, Zhao H, Kushner PJ, Fernandes R (2012) Using models and satellite observations to evaluate the strength of snow albedo feedback. *Journal of Geophysical Research*, **117**, D11117, doi: 10.1029/2012JD017724.

Forbes BC, Fauria MM, Zetterberg P (2010) Russian Arctic warming and "greening" are closely tracked by tundra shrub willows. *Global Change Biology*, **16**, 1542–1554.

Gamache I, Payette S (2004) Height growth response of tree line black spruce to recent climate warming across the forest-tundra of eastern Canada. *Journal of Ecology*, **92**, 835–845.

Hall A, Qu X (2006) Using the current seasonal cycle to constrain snow albedo feedback in future climate change. *Geophysical Research Letters*, **33**, L03502.

Hansen MC, DeFries RS, Townshend J, Carroll M, Dimiceli C, Sohlberg RA (2003) Global percent tree cover at a spatial resolution of 500 meters: first results of the MODIS vegetation continuous fields algorithm. *Earth Interactions*, **7**, 1–15.

Jin Y, Randerson JT, Goetz SJ, Beck PSA, Loranty MM, Goulden ML (2012a) The influence of burn severity on postfire vegetation recovery and albedo change during early succession in North American boreal forests. *Journal of Geophysical Research*, **117**, G01036, doi: 10.1029/2011JG001886.

Jin Y, Randerson JT, Goulden ML, Goetz SJ (2012b) Post-fire changes in net shortwave radiation along a latitudinal gradient in boreal North America. *Geophysical Research Letters*, **39**, L13403.

Kelly R, Chipman ML, Higuera PE, Stefanova I, Brubaker LB, Hu FS (2013) Recent burning of boreal forests exceeds fire regime limits of the past 10,000 years. *Proceedings of the National Academy of Sciences*, **110**, 13055–13060.

Lawrence DM, Swenson SC (2011) Permafrost response to increasing Arctic shrub abundance depends on the relative influence of shrubs on local soil cooling versus large-scale climate warming. *Environmental Research Letters*, **6**, 045504.

Lee X, Goulden ML, Hollinger DY *et al*. (2011) Observed increase in local cooling effect of deforestation at higher latitudes. *Nature*, **479**, 384–387.

Loranty MM, Goetz SJ, Beck PSA (2011) Tundra vegetation effects on pan-Arctic albedo. *Environmental Research Letters*, **6**, 024014.

Macias-Fauria M, Forbes BC, Zetterberg P, Kumpula T (2012) Eurasian Arctic greening reveals teleconnections and the potential for structurally novel ecosystems. *Nature Climate Change*, **2**, 1–6.

Mamet SD, Kershaw GP (2011) Subarctic and alpine tree line dynamics during the last 400 years in north-western and central Canada. *Journal of Biogeography*, **39**, 855–868.

Matthes H, Rinke A, Miller PA, Kuhry P, Dethloff K, Wolf A (2011) Sensitivity of high-resolution Arctic regional climate model projections to different implementations of land surface processes. *Climatic Change*, **111**, 197–214.

O'Halloran TL, Law BE, Goulden ML *et al*. (2012) Radiative forcing of natural forest disturbances. *Global Change Biology*, **18**, 555–565.

Pearson RG, Phillips SJ, Loranty MM, Beck PS, Damoulas T, Knight SJ, Goetz SJ (2013) Shifts in Arctic vegetation and associated feedbacks under climate change. *Nature Climate Change*, **3**, 673–677, doi:10.1038/nclimate1858.

Qu X, Hall A (2007) What controls the strength of snow-albedo feedback? *Journal of Climate*, **20**, 3971–3981.

Qu X, Hall A (2013) On the persistent spread in snow-albedo feedback. *Climate Dynamics*, 1–13.

R Development Core Team (2012) *R: A Language and Environment for Statistical Computing*. R Foundation for Statistical Computing, Vienna. ISBN 3-900051-07-0, URL http://www.R-project.org/.

Randerson JT, Hoffman FM, Thornton PE *et al*. (2009) Systematic assessment of terrestrial biogeochemistry in coupled climate-carbon models. *Global Change Biology*, **15**, 2462–2484.

Ranson KJ, Montesano PM, Nelson R (2011) Object-based mapping of the circumpolar taiga–tundra ecotone with MODIS tree cover. *Remote Sensing of Environment*, **115**, 3670–3680.

Rogers BM, Randerson JT, Bonan GB (2013) High-latitude cooling associated with landscape changes from North American boreal forest fires. *Biogeosciences*, **10**, 699–718.

Schaaf C, Gao F, Strahler A *et al*. (2002) First operational BRDF, albedo and nadir reflectance products from MODIS. *Remote Sensing of Environment*, **83**, 135–148.

Schuur EAG, Vogel JG, Crummer KG, Lee H, Sickman JO, Osterkamp TE (2009) The effect of permafrost thaw on old carbon release and net carbon exchange from tundra. *Nature*, **459**, 556–559.

Serreze MC, Barry RG (2011) Processes and impacts of Arctic amplification: a research synthesis. *Global and Planetary Change*, **77**, 85–96.

Sturm M, Racine C, Tape K (2001) Climate change. Increasing shrub abundance in the Arctic. *Nature*, **411**, 546–547.

Sturm M, Douglas T, Racine C, Liston G (2005) Changing snow and shrub conditions affect albedo with global implications. *Journal of Geophysical Research*, **110**, G01004.

Tape K, Sturm M, Racine C (2006) The evidence for shrub expansion in Northern Alaska and the Pan-Arctic. *Global Change Biology*, **12**, 686–702.

Taylor KE, Stouffer RJ, Meehl GA (2012) An Overview of CMIP5 and the Experiment Design. *Bulletin of the American Meteorological Society*, **93**, 485–498.

Thompson C, Beringer J, Chapin FS III, McGuire A, Franklin J (2004) Structural complexity and land-surface energy exchange along a gradient from arctic tundra to boreal forest. *Journal of Vegetation Science*, **15**, 397–406.

Turetsky MR, Kane ES, Harden JW, Ottmar RD, Manies KL, Hoy E, Kasischke ES (2010) Recent acceleration of biomass burning and carbon losses in Alaskan forests and peatlands. *Nature Geoscience*, **3**, 1–5.

Walker D, Raynolds M, Daniëls F *et al.* (2005) The Circumpolar Arctic vegetation map. *Journal of Vegetation Science*, **16**, 267–282.

Wilmking M, Juday GP, Terwilliger M, Barber VA (2006) Modeling spatial variability of white spruce (Picea glauca) growth responses to climate change at and below treeline in Alaska—A case study from two National Parks. *Erdkunde*, **60**, 113–126.

Supporting Information

Additional Supporting Information may be found in the online version of this article:

Figure S1. Tree cover (A), April (B) and July (C) albedo from MODIS and the CMIP5 models for the study domain. The models are arranged in order of increasing tree cover. Model numbers are given in Table 1.
Figure S2. Map of the study domain showing variability in tree cover with treeline shown in black and distance to treeline transects (Figs S3–S9) outlined in red.
Figure S3. Variability in tree cover, mean July–August NDVI and elevation as a function of distance from treeline (top panel). Proportional land cover classes for the sample area (middle panel), and variability in April, May and July albedo as a function of distance from treeline (bottom panel). Data are for the Eastern Yakutiatransect shown in Fig. S2.
Figure S4. Same as Figure S3, but for the Western Yakutia sample transect (Fig. S2).
Figure S5. Same as Figure S3, but for the Yamaliasample transect (Fig. S2).
Figure S6. Same as Figure S3, but for the Nenetsia sample transect (Fig. S2).
Figure S7. Same as Figure S3, but for the Quebec sample transect (Fig. S2).
Figure S8. Same as Figure S3, but for the Northwest Territories sample transect (Fig. S2).
Figure S9. Same as Figure S3, but for the Alaska sample transect (Fig. S2).
Figure S10. Relationship between fractional tree cover and April albedo for MODIS and CMIP5 models.
Figure S11. Relationship between fractional tree cover and July albedo for MODIS and CMIP5 models.
Figure S12. Relationship between percent canopy cover and April–July Seasonal Albedo Change for MODIS data at 500 m resolution (black line) and mean of MODIS data aggregated to CMIP5 model resolution for each model used in this study (red line). Data are aggregated to nearest percent tree cover, and shaded areas represent interquartile ranges.
Table S1. Model parameters and fit statistics for non-linear relationship between fractional canopy cover and albedo. The model is an exponential decay function in the form $y = ae^{-bx}$. Parameters for models that were not significant (ns, $P > 0.1$) are not reported.